A Novel Power Failure Compensation Control Method for Active Magnetic Bearings Used in High-Speed Permanent Magnet Motor

Gang Liu and Kun Mao

***Abstract*—Active magnetic bearings (AMBs) have been proved superior to conventional bearings in many ways. However, the AMB system will lose magnetic force if the power fails which may cause fatal damage to the rotor and the backup bearings. In order to improve the reliability of the AMB system, a power failure compensation control (PFCC) method is proposed in this paper. A novel hardware composition of PFCC is designed to cooperate with the motor drives using either pulse-width modulation (PWM) or pulse-amplitude modulation techniques. Once the power fails, the motor works as a generator and the back electromotive force (back EMF) is rectified by the antiparallel diodes of the inverter. Meanwhile, a buck converter is utilized to convert the voltage from dc-link of the inverter to the supply voltage for the AMB system. When the motor speed is too low to supply high back EMF for the buck converter, the switches of the inverter are used to boost the dc-link voltage with the motor windings. Furthermore, a hybrid controller combining sliding mode control with PID algorithm is introduced to improve the transient response of the buck converter. Several experimental results confirm the feasibility and effectiveness of the proposed method.**

***Index Terms*—Active magnetic bearing (AMB), buck converter, high-speed permanent magnet (PM) motor, power failure compensation control (PFCC), sliding mode control (SMC).**

I. Introduction

With the fast development of the active magnetic bearing (AMB) technology, more and more high-speed permanent magnet (PM) motors equipped with the AMB systems have been used in industrial applications such as inertia momentum wheel [1], [2], control moment gyroscope [3], [4], turbine machinery [5], flywheel energy storage system (FESS) [6]–[9], etc. Despite many advantages over the conventional bearings including active vibration control, no contact, and no lubrication, the AMB system needs the electrical power to generate the magnetic force for suspending rotor [10]. In fact, several different reasons, such as the mains power system overcurrent, may cause the power failure of the AMB system. Meanwhile, the AMB system cannot generate its magnetic force to support the rotor without proper power failure compensation control (PFCC) method. Moreover, if the motor is running at high speed, the rotor will decelerate dramatically when it touches down the backup bearings, which may bring fatal damage to the rotor laminations and the backup bearings [11]. Therefore, the PFCC method is a critical issue to improve the reliability of the AMB system.

The uninterrupted power supply (UPS) based on the backup batteries is popular and efficient for the AMB system to prevent damage from the mains power failure. However, the backup batteries are sensitive to the working environment such as temperature and humidity. Despite many studies have been carried out in the last decades, and some useful conclusions are given to improve the performance of batteries [12]–[14]. Due to the regular maintenance of the UPS, the whole cost of the AMB system will increase significantly [15]. In order to overcome the shortcomings of backup batteries, the kinetic energy conversion of rotor is an ideal solution for the AMB system because of its compactness, high efficiency, and less maintenance [16], [17]. When the mains power failure occurs, the motor works as a generator and the kinetic energy will be the feedback to the dc-link. Apparently, the working principle of the PFCC method is much like FESS which has been studied during the last decades for its pollution free and high efficiency. Since the efficiency of the energy conversion is the key issue for the FESS, the backup battery is still needed to prevent mains power failure if the AMB system is equipped [18]–[20]. Actually, the response time of changing the mains power supply of the AMB system to the backup one is very rigorous. The regenerative braking of the electric vehicles and hybrid electric vehicles also has the similar kinetic energy feedback process [21]–[24]. However, the regenerative braking systems are designed to distribute the braking force efficiently by controlling the motor currents. Besides, the voltage of the dc-link is not controlled actively during motor braking process, which may cause the dramatically oscillation of the dc-link voltage. In [25] and [26], only one flyback-type offline dc/dc converter which provides the power supply for the whole system is inserted between the dc-link of the inverter and the AMB system. Since the offline dc/dc converter works all the time, the power failure detection circuit is not necessary. Because of its simplicity and effectiveness, the offline dc/dc converter is usually analyzed with its small-signal model and designed based on the power control integrated chips (ICs). With the development of the dc/dc control technologies, many kinds of them have been successfully applied in the power control ICs including the voltage mode control [27], current mode control [28], etc.

Manuscript received April 28, 2015; revised June 30, 2015; accepted August 11, 2015. Date of publication August 21, 2015; date of current version January 7, 2016. This work was supported in part by the National Nature Science Funds of China under Grant 61374029 and in part by the National Major Project for the Development and Application of Scientific Instrument Equipment of China under Grant 2012YQ040235. Recommended for publication by Associate Editor F. Wang.

The authors are with the the College of Instrumentation Science and Optoelectronics Engineering, BeiHang University, Beijing 100191, China (e-mail: lgang@buaa.edu.cn; maokun_buaa@163.com).

Color versions of one or more of the figures in this paper are available online at http://ieeexplore.ieee.org.

Digital Object Identifier 10.1109/TPEL.2015.2471807

Due to the nonlinearity and parameter time-varying characteristics of the dc/dc converter, it is difficult for these linear control technologies to compensate output voltage variation when large signal disturbance occurs [29]–[31]. In order to overcome these shortcomings, practical nonlinearity control technologies of the dc/dc converter have been studied in recent years, especially on charge balance control [32] and sliding mode control (SMC) [33]. Because of its simplicity, SMC is very suitable for the dc/dc switching converter control to improve the transient response. However, the steady-state accuracy is limited due to the nonideal switching frequency and chattering problem [34]. With the development of digital signal processor, more and more digital dc/dc switching converter controllers are implemented with low cost. Because of the high flexibility of control software, the performance of the dc/dc switching converter can be greatly improved by taking advantage of the digital controller composed of both the linear and nonlinear control algorithm [35].

This paper proposes a PFCC method which is fully integrated with high-speed PM motor drive. In order to make it suitable for the motor drives using either pulse-width modulation (PWM) or pulse-amplitude modulation (PAM) control methods, a novel hardware composition of PFCC method including the ac/dc converter, high voltage (HV) dc/dc converter, and low voltage (LV) dc/dc converter is designed first. A hybrid controller combined SMC with PID algorithm is also introduced to improve the transient response of the HV buck converter. Therefore, the remainder of the paper is organized as follows: The previously reported power failure control method for the AMB system and the improved power failure compensation device are compared in Section II. In order to improve the transient response of the HV dc/dc converter, a hybrid controller composed of SMC and PID algorithm is proposed in Section III. It is shown that the efficiency of kinetic energy conversion can be greatly improved by using the switches of the inverter to boost the dc-link voltage when the rotor is running at low speed. This is given in Section IV. The experiment results are shown to validate the proposed PFCC method in Section V. At last, Section VI concludes this paper.

II. Hardware Composition of the PFCC Method

A. Review of Hardware Composition for Power Failure Compensation

The basic hardware composition of the AMB system shown in Fig. 1 has been widely used. When the mains power failure occurs, the ac/dc converter stops working and the rotor touches down the backup bearings without electromagnetic force. Because of its high efficiency and less maintenance, the control method of compensating power failure based on the kinetic energy conversion has been studied and the typical hardware composition is shown in Fig. 2 [26]. Only one offline dc/dc converter is inserted between the dc-link and the AMB system controller which provides the electrical power during the whole working time. When the mains power fails, the back EMF of the motor is rectified by the antiparallel diodes of the inverter, and the electrical power of the whole control system circuits are supplied by the offline dc/dc converter. The offline dc/dc converter

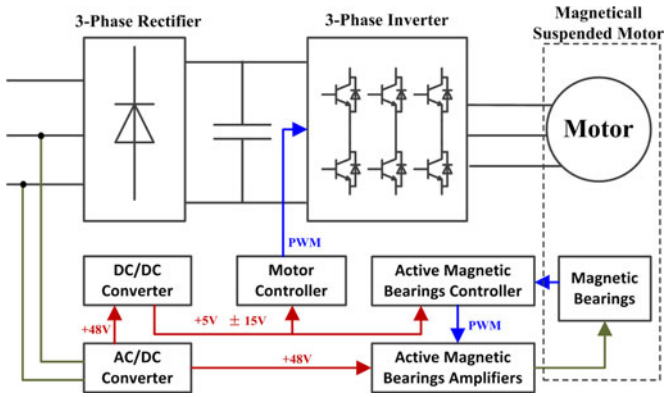

Fig. 1. Diagram of motor drive and AMB control circuits.

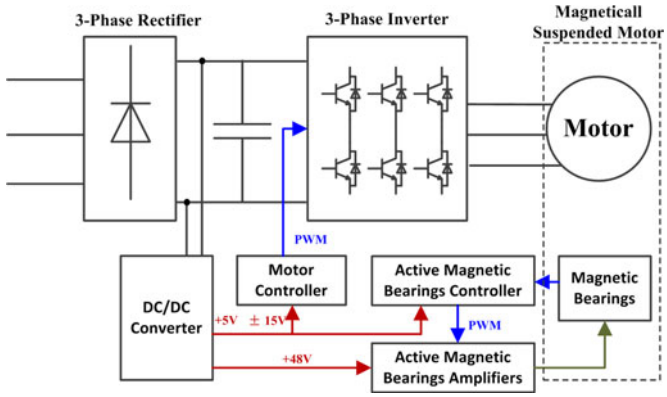

Fig. 2. Diagram of motor drive and AMB control circuits with capability of power failure compensation.

is easy to be integrated with the motor drive using PWM control method because of its simplicity of hardware implementation. However, more and more drives of high-speed PM motors use PAM control strategy to improve efficiency by reducing the loss of motors [36], [37]. Due to the small value of the dc-link voltage, when the drive uses PAM control strategy to start motor, the offline dc/dc converters may fail to supply electrical power for the control system.

B. Proposed Hardware Composition of PFCC

In order to overcome the disadvantages of the PFCC method reported previously, a novel hardware composition of PFCC is proposed as shown in Fig. 3. The improved PFCC hardware is composed of the power failure detection circuit, ac/dc converter, HV dc/dc converter, and LV dc/dc converter. The ac/dc converter provides +48 V as the mains power for the AMB system and the LV dc/dc converter. The LV dc/dc converter provides +5 V and ±15 V for the motor drive control circuit. In order to increase the system reliability, the LV dc/dc converter is composed of the isolated brick-type dc/dc converters. Because of its reliability and simplicity, the offline ac/dc converter is chosen as the mains power supply while the HV dc/dc converter is utilized to compensate the power failure. In order to reduce the response time, the HV dc/dc converter control algorithm and

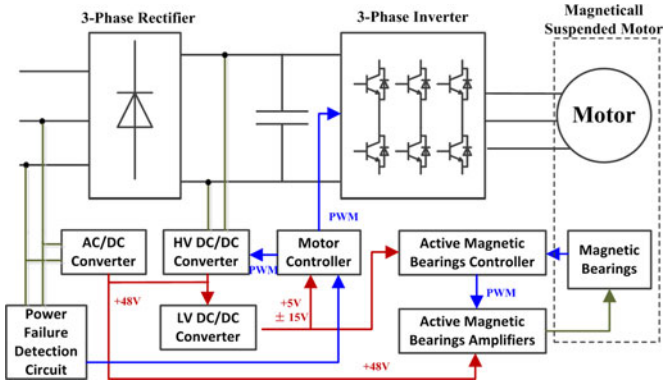

Fig. 3. Diagram of motor drive and AMB control circuits with the proposed PFCC method.

the power failure detection function are all integrated with the motor drive software. The buck-type converter is selected for its high efficiency and simple mathematical model for digital control [35]. Also, a hybrid controller composed of SMC and PID algorithm is designed to improve the transient response and reduce the steady-state error without increasing software complexity significantly.

Therefore, the hardware of the proposed PFCC method has some advantages over the traditional PFCC method as shown in Fig. 2. First, the proposed PFCC method can cooperate well with the drives using both PAM and PWM technology, while the PFCC method described in Fig. 2 can only work with the drives using PWM technology. Second, the HV dc/dc can work as a backup circuit to provide power for the control system if the offline ac/dc converter fails. However, the control system, which is depicted in Fig. 2, will lose its power supply if the dc/dc converter fails for some hardware problems. Finally, the HV dc/dc converter can be controlled according to the running condition of the motor. For example, in the vacuum applications, the deceleration of the magnetically levitated rotor usually requires a power resistor to dissipate the kinetic energy of the rotor. If the proposed PFCC method is used, the HV dc/dc converter can be used to replace the ac/dc converter by providing a little higher output voltage when the motor is braking. At this time, the kinetic energy of the rotor is converted to the power supply for the control system and the power resistor is no longer needed.

The back EMF of the motor is rectified by antiparallel diodes and all switches of the inverter are turned OFF when the speed is high enough to make the buck-type HV dc/dc converter work. Otherwise, the switches of the inverter are utilized to boost the back EMF with the motor windings.

The kinetic energy of a rotating rotor E can be expressed as

$$E = \frac{1}{2} J\omega^2 \tag{1}$$

where J is the moment of inertia and ω is the speed of the rotor.

When the rotor touches down the backup bearings, the rotor decelerates dramatically and most kinetic energy is converted to the thermal energy by friction. The kinetic energy of the rotor can be expressed as

$$E_t = \frac{1}{2} J\omega_t^2 = P_t + P_o \tag{2}$$

where ω_t is touchdown speed, P_t is frictional thermal energy, and P_o is other kind of the dissipated energy. Since the kinetic energy conversion efficiency is improved with a low touchdown speed, the damage of the rotor laminations and the backup bearings can be greatly reduced.

III. Implementation of the HV DC/DC Converter

As mentioned earlier, the buck-type HV dc/dc converter is the key component of the PFCC hardware composition. In spite of simple implementation for the linear controller such as the PID regulator, further improvement of the dc/dc switching converter transient response under large signal disturbance is limited. As shown in Figs. 2 and 3, the load of the dc/dc converter consists of the AMB windings and its drives. The equivalent load type is more complex than just resistance. In addition, it has a close relationship with the inductance of the AMB windings and the current dynamic response of the drives. As the centrifugal force increases in accordance with the rotational frequency of rotor, the AMB drives have to provide more control current to suppress the unbalanced rotor displacement which decays the current dynamic performance. Hence, the load model of the AMBs control system is nonlinear and related to the rotor rotation state. Due to the nonlinear nature of the dc/dc switching converter and the load, the SMC method can significantly improve the robustness and transient response in contrast with PID regulator. Furthermore, it does not require the precise load model information for the dc–dc converter control, and the model with resistive load works sufficiently well. However, it is hard for SMC to decrease the steady-state error because of its chattering problem [33]. Meanwhile, the dc/dc switching converter using the PID regulator can get satisfying steady-state accuracy with proper parameters. Therefore, a hybrid controller composed of SMC and PID algorithm is designed to control the buck-type HV dc/dc converter in this section.

A. Control Model of the Buck Converter

The SMC controller is active when output voltage error exceeds specified threshold, otherwise the PID regulator is used. In order to simplify analysis, the buck converter is designed to work in continuous conduction mode (CCM) with proper buck converter parameters.

The output voltage feedback control model of the buck-type HV dc/dc converter is shown in Fig. 4. When the buck converter works in CCM, the output voltage error x_1 and its rate x_2 can be expressed as

$$\begin{cases} x_1 = v_{\text{ref}} - \beta v_o \\ x_2 = \dot{x}_1 = -\beta \dfrac{dv_o}{dt} = \dfrac{\beta}{C}\left(\dfrac{v_o}{R_L} - \displaystyle\int \dfrac{u \cdot v_i - v_o}{L} dt\right). \end{cases} \tag{3}$$

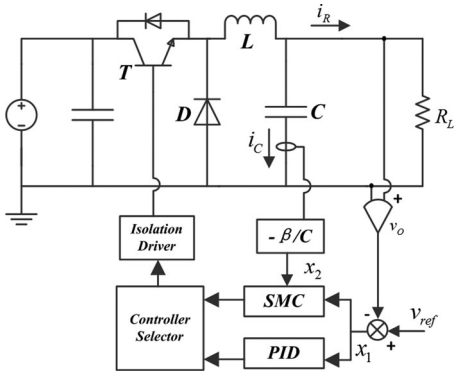

Fig. 4. Diagram of proposed buck converter controller.

The differentiation of x_2 can be expressed as

$$\begin{aligned}\dot{x}_2 &= \frac{\beta}{C}\cdot\frac{1}{R_L}\cdot\frac{dv_o}{dt} - \frac{\beta}{C}\left(\frac{u\cdot v_i - v_o}{L}\right)\\ &= \frac{1}{R_L C}\cdot\beta\cdot\frac{dv_o}{dt} - \frac{\beta v_i}{LC}\cdot u + \frac{\beta}{LC}\cdot v_o\\ &= -\frac{1}{R_L C}\cdot x_2 - \frac{\beta v_i}{LC}\cdot u + \frac{v_{\rm ref}}{LC} - \frac{v_{\rm ref}}{LC} + \frac{\beta}{LC}\cdot v_o\\ &= -\frac{1}{R_L C}\cdot x_2 - \frac{v_{\rm ref}}{LC} + \frac{\beta}{LC}\cdot v_o - \frac{\beta v_i}{LC}\cdot u + \frac{v_{\rm ref}}{LC}\\ &= -\frac{1}{R_L C}\cdot x_2 - \frac{1}{LC}(v_{\rm ref} - \beta v_o) - \frac{\beta v_i}{LC}\cdot u + \frac{v_{\rm ref}}{LC}\\ &= -\frac{1}{R_L C}\cdot x_2 - \frac{1}{LC}\cdot x_1 - \frac{\beta v_i}{LC}\cdot u + \frac{v_{\rm ref}}{LC}. \end{aligned} \tag{4}$$

Therefore, the state-space model of the buck converter can be described as

$$\begin{bmatrix}\dot{x}_1\\ \dot{x}_2\end{bmatrix} = \begin{bmatrix}0 & 1\\ -\dfrac{1}{LC} & -\dfrac{1}{R_L C}\end{bmatrix}\begin{bmatrix}x_1\\ x_2\end{bmatrix} + \begin{bmatrix}0\\ -\dfrac{\beta v_i}{LC}\end{bmatrix}u + \begin{bmatrix}0\\ \dfrac{v_{\rm ref}}{LC}\end{bmatrix} \tag{5}$$

where $v_{\rm ref}$ is the input reference voltage, β is the feedback coefficient of the output voltage, v_i is the input voltage of the buck converter, v_o is output voltage of the buck converter, C is capacitance of the buck converter, R_L is equivalent load resistance, L is inductance of the buck converter, u is 1 when the switch turns ON and 0 when the switch turns OFF.

B. SMC Controller Design

The SMC voltage controller is activated when the output voltage error exceeds the specified threshold. Due to the limitation of the nonideal hardware implementation, the switching frequency of the SMC controller cannot be too high. The hysteresis-type SMC controller has been proved to be able to reduce the switching frequency effectively [33]. The control law can be expressed as

$$u_s = \begin{cases} 1 & \text{switch ON, when } s > k\\ 0 & \text{switch OFF, when } s < -k\\ & \text{no change,when } -k \le s \le k\end{cases} \tag{6}$$

where k indicates hysteresis band. The sliding surface s can be defined as

$$s = \alpha x_1 + x_2 \tag{7}$$

where α indicates the coefficient of SMC. It is very important to choose α which affects the stability and dynamic performance of SMC significantly. According to [33], it is sufficient to set $\alpha = 1/r_{\rm LC}$ for fast dynamic response and maintaining a large existence region. The hysteresis band k can be expressed as

$$k = v_{\rm ref}\left(1 - \frac{v_{\rm ref}}{v_i}\right)/(2f_{\rm sd}L) \tag{8}$$

where $f_{\rm sd}$ is the expectation value of the steady-state switching frequency.

C. PID Controller Design

The PID controller is activated when the output voltage error is below the specified threshold. The parameters can be tuned by using the pole-zero assignment method while the control law is described as

$$u_p = k_p\cdot x_1 + k_i\int x_1 dt + k_d\cdot\frac{dx_1}{dt} \tag{9}$$

where k_p is the proportional gain, k_i is the integration gain, and k_d is the differential gain.

IV. Control Strategy of Back EMF

The line-to-line back EMF of the PM motor can be expressed as

$$e_{ab} = k_e\cdot p\cdot\omega \tag{10}$$

where k_e indicates the coefficient of the line-to-line back EMF, p is the pole pairs of the motor, and ω is the rotor speed.

As mentioned earlier, the HV dc/dc converter cannot work when the speed is too low to generate enough high line-to-line back EMF. Therefore, the flyback-type dc/dc converter which could lower or boost the input voltage is used as the HV dc/dc converter as shown in Fig. 2. However, there are two problems of the flyback-type dc/dc converter. First, the magnetic forces of the AMB systems are limited by the output power of the flyback-type converter which is usually below 200 W. Second, the efficiency of the flyback-type dc/dc converter dramatically decreases when the switching duty ratio is too high or too low. The buck converter is selected as the HV dc/dc converter for its high efficiency. However, the output voltage of the buck converter is limited by the input voltage. In order to make buck converter work in a wide speed range, a novel control strategy of back EMF is proposed.

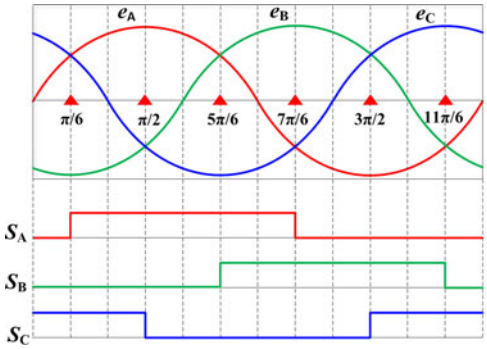

Fig. 5. Relationship between phase back EMF of PM motor and rotor position. S_A, S_B, and S_C are the ideal electrical angle signals which can be got by position sensor such as hall sensor or sensorless strategy.

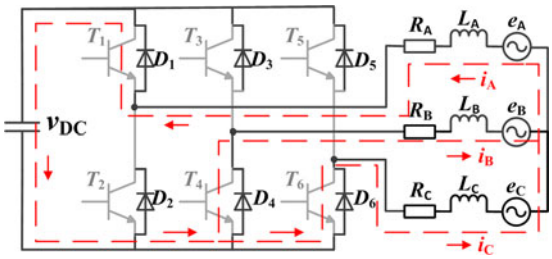

Fig. 6. Current flowing path if electrical angle θ is from pi/6 to 5 pi/6 when switches are turned OFF.

A. Control Strategy of Back EMF When Rotor Speed is High

The buck-type HV dc/dc converter works as soon as the mains power supply fails. When the dc-link voltage is high enough to keep the buck-type HV dc/dc working, the switches of the inverter are turned OFF and the back EMF of the motor is rectified by the antiparallel diodes. For facilitate analysis, the phase back EMF with the position information is shown as Fig. 5. When the electrical angle θ is from pi/6 to 5 pi/6, the current flowing path can be depicted as Fig. 6. Therefore, the value of the dc-link voltage $v_{\rm dc}$ can be expressed as

$$v_{\rm dc} = \sqrt{2} \cdot e_{ab} \approx 1.414 \cdot k_e \cdot \omega. \tag{11}$$

Apparently, the dc-link voltage is proportional to the amplitude of the line-to-line back EMF.

B. Control Strategy of Back EMF When Rotor Speed is Low

The buck-type HV dc/dc converter will stop working when the dc-link voltage is not high enough. The PWM rectified method based on six controllable switches is a practical approach. However, the rotor position information with high revolution is necessary for this control method which makes it hard to be integrated with PM motor drive based on three-hall position sensors or sensorless control strategy.

In order to improve the efficiency of the energy conversion, the control strategy of the back EMF is proposed to regulate the dc-link voltage actively without high-resolution position information. When the electrical angle θ is from pi/6 to pi/2, the

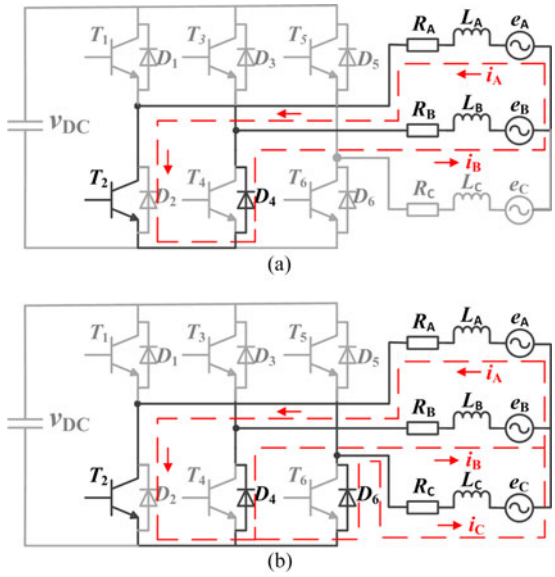

Fig. 7. Current flowing path when T2 is turned ON. (a) $e_c > 0$. (b) $e_c < 0$.

switches T_1, T_3, T_5, T_4, and T_6 are turned OFF and T_2 is controlled by PWM. The principle can be described as following:

1) T_2 is Turned ON: If $e_c > 0$, the antiparallel diodes D5 and D6 are shut OFF, while D4 is ON. From Fig. 7(a), the current flows through phase A, T2, D4, and phase B. The line-to-line back EMF $e_{\rm AB}$ provides the currents for the windings of phase A and B, while the current of phase A is equal to the current of phase B. The increased energy of inductors could be expressed as $W = 0.5 \cdot L \cdot I^2$. The magnetic energy stored in windings of phase A and B is increased gradually. If $e_c < 0$, the antiparallel diodes D4 and D6 are turned ON, while the D5 is still shut OFF. From Fig. 7(b), the current flows through all three phase windings. The line-to-line back EMF $e_{\rm AB}$ and $e_{\rm AC}$ provide the currents for all three phase windings. The current of phase A is equal to the sum of the other two phase currents. At this time, the magnetic energy of phase A and B are still increased, while the rate is gradually decreased. The magnetic energy of phase C starts to increase and the rate is faster than the other two phases. At this time, most of the kinetic energy is stored as magnetic energy and the remainder energy is dissipated as the thermal type.

2) T2 is Turned OFF: A high EMF of the motor winding is generated when T2 is shut OFF. The magnetic energy stored in the phase windings is reversed to the dc-link capacitor which steps up the dc-link voltage. At this time, the current flows through phase A, D1, dc-link capacitor, D4, and phase B as shown in Fig. 8.

When θ equals to other value, the relationship between θ and active switch can be given in Table I. Although different switch is controlled according to the rotor position information, there is only one switch activated at any time which makes the control strategy easy to realize. Besides, only six discrete electrical angles are needed, which makes the control strategy of the EMF easy to be integrated with the PM motor drive system using low-resolution position sensors or sensorless control strategy.

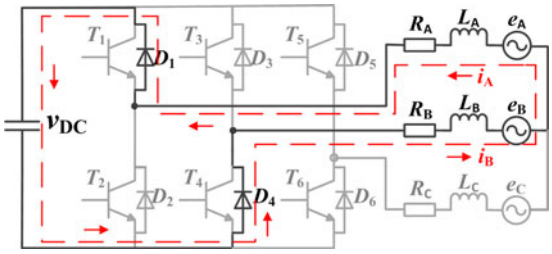

Fig. 8. Current flowing path when T2 is turned OFF.

TABLE I
ACTIVE SWITCH ACCORDING TO ELECTRICAL ANGLES

Electical Angle θ	Active Switch
$[\pi/6, \pi/2)$	T_2
$[\pi/2, 5\pi/6)$	T_6
$[5\pi/6, 7\pi/6)$	T_6
$[7\pi/6, 2\pi/3)$	T_4
$[2\pi/3, 11\pi/6)$	T_4
$[11\pi/6, \pi/6)$	T_2

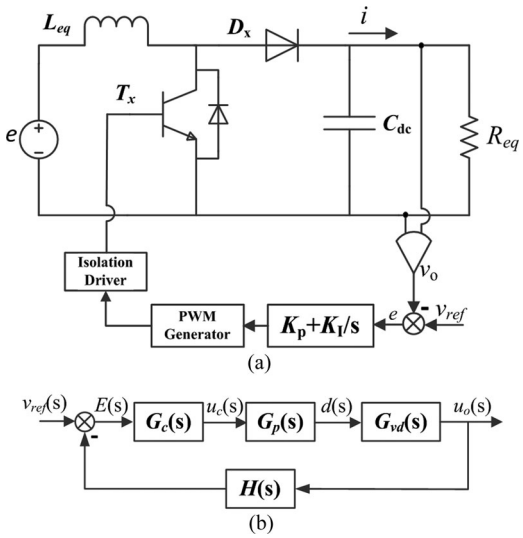

Fig. 9. Diagram of equivalent boost converter. (a) Circuit diagram of the boost converter. (b) Control diagram of the boost converter.

As mentioned earlier, the system works as a boost dc/dc converter. The fast transient response of the boost converter is not necessary because the output voltage is supplied for the HV dc–dc converter input. The hybrid controller of the HV dc–dc converter is used to improve the voltage supply for the AMB system. In addition, the proposed back EMF strategy only works when the motor runs at low speed. Hence, a simple PI controller based on the small signal model of the boost converter is utilized to realize the voltage output feedback control. The system circuit and control diagram is depicted as Fig. 9. The equivalent inductor $L_{\rm eq}$ is the sum value of two phase windings self-inductor. According to the different value of θ, T_x could be T_2, T_4, or T_6 while the corresponding D_x is D_1, D_3, or D_5. The output

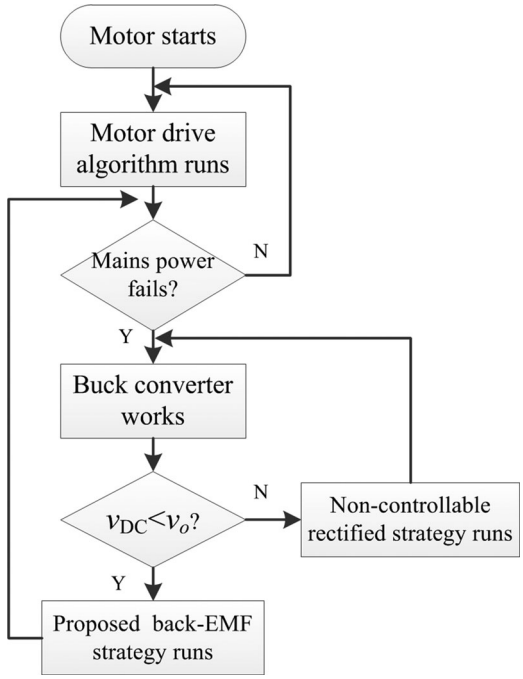

Fig. 10. Control flow of proposed PFCC method.

capacitor of the equivalent boost dc/dc converter is the dc-link capacitor of the motor drive. Since the $L_{\rm eq}$ is constant, the value of dc-link capacitor should be as large as possible to reduce the dc-link voltage ripple with limitation of cost and volume.

According to [33], the transfer function from PWM control duty ratio d(s) to output voltage u_o(s) is expressed as $G_{vd}(s) = \frac{d' \cdot U_o \cdot (1 - Ls/(Rd'^2))}{LCs^2 + Ls/R + d'^2}$ where $d' = 1 - d$ and d is PWM control duty ratio. $H(s)$ is the transfer function of the boost control system feedback part and could be given as a proportional element $H(s) = K_F$. The PI controller transfer function G_c(s) can be expressed as $G_c = K_p + K_I/s$.$G_p(s)$ is the transfer function of PWM modulator and a proportional element K_s could be a satisfactory approximation.

C. Proposed PFCC Method Incorporated With Motor Drive

As mentioned earlier, the control flow of the proposed PFCC method incorporated with drive algorithm can be shown in Fig. 10. When the start signal is given, the motor drive algorithm runs immediately, and the mains power is monitored at fix sample period. Once the mains power failure happens, the PFCC strategy is activated and the buck converter works immediately. If the input $v_{\rm dc}$ of buck converter is higher than output value v_o, the noncontrollable rectified strategy is chosen to simplify control software. Otherwise, the proposed active back EMF control strategy is used.

V. EXPERIMENTAL EVALUATION

A. Experiment Setup

The experiments about the proposed PFCC method have been successfully implemented on the magnetically levitated

TABLE II
MOTOR PARAMETERS

High-Speed BLDC Motor	
Rated power, P_N	1.4 kW
Rated dc voltage, V_N	100 V
Rated speed, ω_N	21 000 r/min
Phase resister, *R*	0.28 Ω
Phase inductance, *L*	0.24 mH
Number of pairs, *P*	2
Line-to-line back EMF constant, K_e	0.0033 V/(r/min)
Moment of inertia, *J*	0.002139 kg·m^2

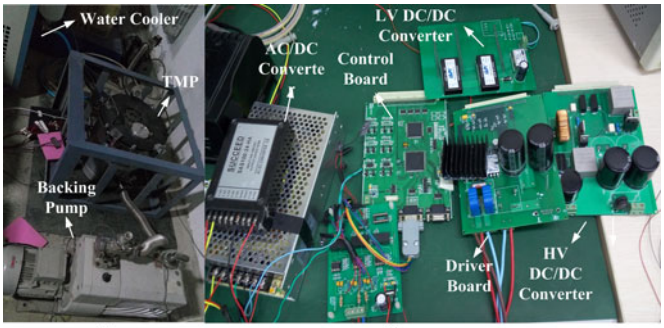

Fig. 11. Experimental platform. (a) Magnetically Levitated TMP Testing System. (b) Motor drive with PFCC hardware.

TABLE III
POWER CONSUMPTION

Practical HV buck-type DC/DC converter Power Consumption		
Motor control circuit	48 V	0.8 A
AMB control circuit	48 V	0.9 A
AMB windings	48 V	1.6 A
Total power, P_N	$P_N = 48(0.8+0.9+1.6) = 160$ W	
Equivalent load resistor, R_{eq}	$R_{eq} = 48/(0.8+0.9+1.6) \approx 14.5\ \Omega$	

high-speed BLDC motor which is used for the turbo molecular pump (TMP). The specification of the experimental high-speed BLDC motor is shown in Table II, and the experimental platform is shown in Fig. 11.

B. Proposed Control Strategy of the Buck Converter Validation

In order to design the buck converter, the power consumption distribution of the motor drive and the AMB control system is carefully tested. The result is shown in Table III. The buck converter is designed to work in CCM mode, and its parameters are shown in Table IV.

According to the principle of proposed PFCC method, the step input response time of the HV buck converter is very crucial to compensate the voltage drop when mains power failure occurs. Since the input voltage of the LV dc/dc converter and AMB windings can vary within a certain range, a high steady-state accuracy of output is not necessary. The step input response comparison of the buck converter using PI regulator and proposed hybrid controller is conducted. The results are shown in Fig. 12.

TABLE IV
CONVERTER PARAMETER

Parameters of HV buck converters	
Inductor, L	1 mH
Capacitor, C	940 μF
Switch Frequency, f_{sd}	10 kHz
Rated output voltage, V_o	48 V
Rated output current, I_o	4 A
Equivalent load resistor, R_L	14.5 Ω
LV DC/DC input, V_{LV}	36–60 V

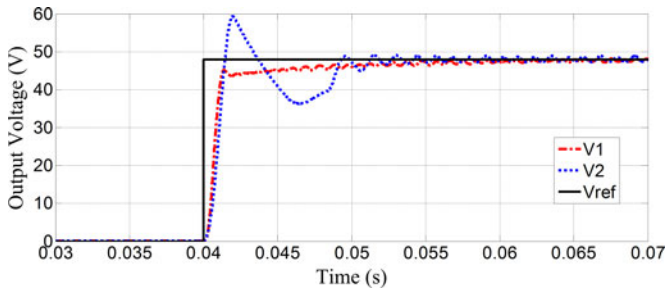

Fig. 12. Step input response of buck converter using PI regulator and proposed hybrid controller. The V1 is output of buck converter using proposed hybrid controller while V2 is output of buck converter using PI controller.

The transient response could be improved by increasing the parameter K_p of the PI controller. However, the over shoot of the output voltage is also increased which may damage the LV dc/dc converter. From Table IV, the maximum input of the LV dc/dc converter is 60 V while the minimum input is 36 V. Therefore, the overshoot of the buck converter should not exceed 25% of the rated value. The PI digital controller is tuned with Ziegler–Nichols method [38]. After trying many different PI coefficients, a good step input responses shown as V2 can be achieved when K_p is 550 and K_i is 1200. The rise time when the output value first exceeds 36 V is about 1 ms and the overshoot is about 11 V. The result with proposed hybrid controller combined SMC with PI algorithm is shown as V1. Although the SMC algorithm is implemented as a digital hysteresis controller with a fixed switching frequency $f_{\rm ad}$ and AD sample time T_s, the step input response time is still much shorter than the PI controller. When the output voltage error of the buck converter is less than 5 V, the PI controller is activated. With a smaller value of proportional coefficients k_p, the over shoot of the output voltage can be eliminated.

C. Control Strategy of Back EMF Validation

Since the high-speed rotor may touch down the backup bearings with unsuited control parameters during PFCC experiments, a power resister is used as the equivalent load of the

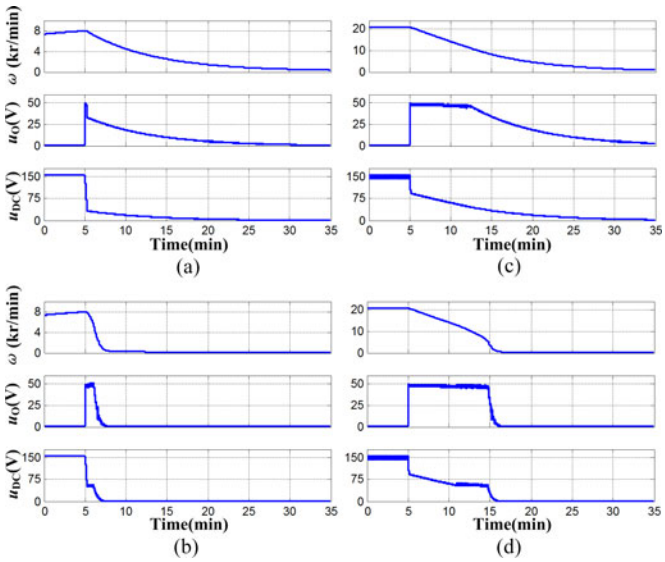

Fig. 13. Experimental results with different back EMF control strategy. (a) Noncontrollable rectified strategy when motor runs at 8000 r/min. (b) Proposed active back EMF strategy when motor runs at 8000 r/min. (c) Noncontrollable rectified strategy when motor runs at 21 000 r/min. (d) proposed active back EMF strategy when motor runs at 21 000 r/min.

buck converter to prevent the potential damage. The reference output voltage of the buck converter is set as +48 V, and a simple output voltage feedback controller using PI algorithm in contrast with proposed control algorithm is integrated with the motor drive software. The controller drives the motor to a fixed speed first. Then, the mains power of motor is shut OFF while the power of control circuits is still ON. The speed of motor, the dc-link voltage, and the output of the buck converter are all monitored.

The motor is speeded up to 8000 r/min first. Then, the mains power of the motor drive is shut OFF while the AMB system power is ON. The experiment result is given in Fig. 13(a). The six IGBTs of inverter are all switched OFF and the back EMF of the motor is rectified by the antiparallel diodes. The dc-link voltage $u_{\rm dc}$ decreases dramatically when the buck converter works. Due to the low speed of motor, the line-to-line back EMF is not high enough to keep the buck converter working for long time steadily. The buck converter works normally for about only 30 s. The motor runs at 7200 r/min when the output voltage of the buck converter is below +36 V. The deceleration lasts about 25 min. As shown in Fig. 13(b), the proposed back EMF control strategy is used when the dc-link voltage is below +55 V. Because of the high efficiency of the energy conversion, the buck converter works for about 1.7 min with a fixed dc-link voltage. The motor decelerates dramatically from 8000 r/min to standstill in 4 min. The touchdown speed is only 4800 r/min.

The similar experiment results are shown in Fig. 13(c) when motor runs at rated speed 21 000 r/min. Without active back EMF control strategy, the buck converter works for 7 min, and the whole deceleration lasts about 35 min. The speed of the rotor is about 7300 r/min when the output voltage of the buck converter is below +36 V. As shown in Fig. 13(d), the buck converter works for 10 min while the deceleration lasts 12 min with proposed back EMF control strategy. The motor runs at about 11 000 r/min when the voltage of dc-link is below +55 V. In addition, the phase currents of motor can be depicted as Fig. 14(a) while the phase currents using noncontrollable rectified method are shown in Fig. 14(b). The motor speed is about 4700 r/min when the output voltage is below +36 V.

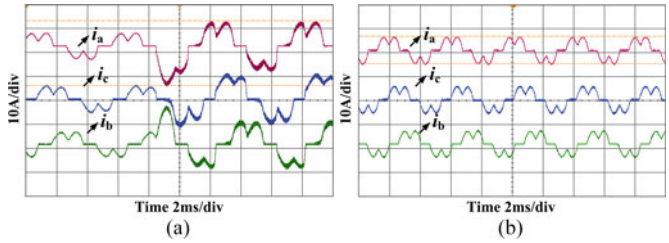

Fig. 14. Motor phase currents using different back EMF control strategy. (a) Proposed-back EMF control strategy. (b) Noncontrollable rectified strategy.

The comparison of the kinetic energy conversion efficiency with different back EMF control strategy can also be conducted. According to (1), the variation of the kinetic energy ΔE while the mains power failure happens can be expressed as

$$\Delta E = \frac{1}{2}J\omega_n^2 - \frac{1}{2}J\omega_t^2 = E_s + E_t \tag{12}$$

where ω_n is the speed of the rotor when the power fails and ω_t is the touchdown speed. E_s is the energy which is converted to electrical power for the motor control circuit and the AMB systems. E_t is other kinds of dissipated energy and the major part is copper consumption. For the small phase resistance of high-speed motor, E_t is far less than E_s. For facility analysis, ΔE is approximately equal to E_s.

The efficiency of the kinetic energy conversion η could be expressed as

$$\begin{aligned}\eta &= \frac{E_s}{0.5\cdot J\omega_n^2}\times 100\% \\ &\approx \frac{\Delta E}{0.5\cdot J\omega_n^2}\times 100\% \\ &= \frac{0.5\cdot J\omega_n^2 - 0.5J\omega_t^2}{0.5\cdot J\omega_n^2}\times 100\% \\ &= \left(1-\frac{\omega_t^2}{\omega_n^2}\right)\times 100\%. \end{aligned} \tag{13}$$

As mentioned earlier, if ω_n is fixed, the efficiency η increases as the touchdown speed ω_t decreases. According to the experimental results, when the motor runs at rated 21 000 r/min, the touchdown speed is about 7300 r/min without the proposed back EMF control strategy. In this case, the efficiency of kinetic energy conversion is about 87.9%. On the other hand, if the proposed back EMF control strategy is used, the touchdown speed is about 4700 r/min, and the efficiency is about 95.0%. Hence, with the numeric comparison, the efficiency of the kinetic

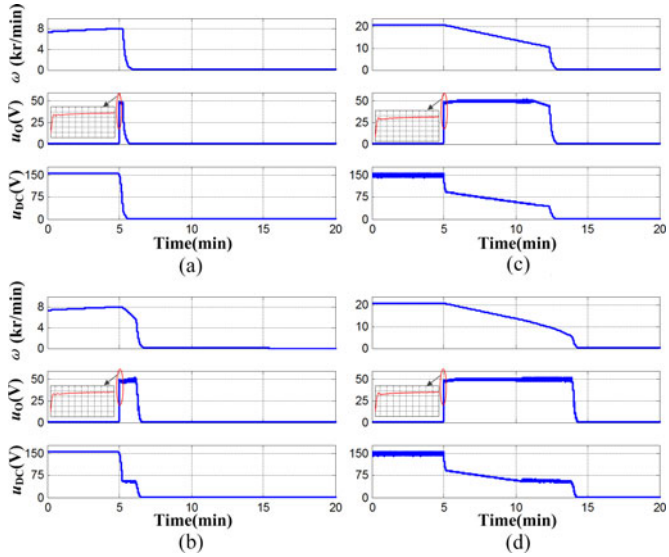

Fig. 15. Experimental results of different PFCC method of AMB system based on hybrid control method. (a) Noncontrollable rectified strategy when motor runs at 8000 r/min. (b) Proposed active back EMF strategy when motor runs at 8000 r/min. (c) Noncontrollable rectified strategy when motor runs at 21 000 r/min. (d) Proposed active back EMF strategy when motor runs at 21 000 r/min.

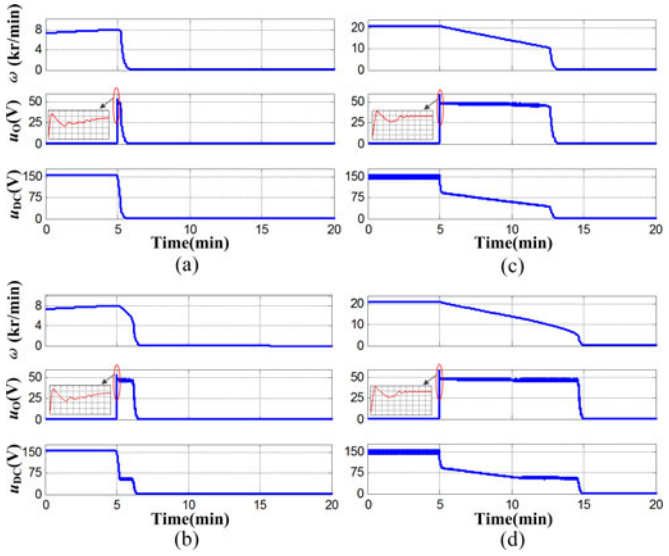

Fig. 16. Experimental results of different PFCC method of AMB system based on PID control method. (a) Noncontrollable rectified strategy when motor runs at 8000 r/min. (b) Proposed active back EMF strategy when motor runs at 8000 r/min. (c) Noncontrollable rectified strategy when motor runs at 21 000 r/min. (d) Proposed active back EMF strategy when motor runs at 21 000 r/min.

energy conversion could be improved by using the proposed back EMF control strategy. The output voltage of the buck converter works longer while the brake time of the motor is greatly reduced which is very helpful for vacuum applications.

D. PFCC Method for AMB System Validation

The proposed PFCC method is implemented on the experimental platform by replacing the power resister with the LV dc/dc converter and AMB system control circuits. The experimental results are shown in Fig. 15.

Once the motor is speeded up to 8000 r/min, the mains power of the experimental platform is shut OFF. As shown in Fig. 15(a), the buck converter works for about 30 s without active control strategy of the back EMF. After that, the AMB system loses its power, and the rotor touches down the backup bearings at 7200 r/min. Due to the friction between the rotor and the backup bearings, the motor decelerates quickly and the whole brake time lasts only 1 min. With the proposed PFCC method, the experiment result is shown in Fig. 15(b). The buck converter works about for 1.5 min before the AMB system loses its power. The touchdown speed is about 5000 r/min, and the whole brake time lasts 2 min.

When the motor is speeded up to 21 000 r/min, the buck converter works for about 7.5 min without active control strategy of back EMF as shown in Fig. 15(c). The touchdown speed is about 8200 r/min, and the whole deceleration lasts for about 8.5 min. With the proposed PFCC method shown in Fig. 15(d), the touchdown speed is only 4600 r/min. The buck converter works for about 12 min which is much longer. With a lower touchdown speed, the kinetic energy of the rotor is much less which decreases the damage of the rotor laminations and the backup bearings.

E. Performance Comparison Between Proposed Hybrid Control Method and PID Controller

The HV dc/dc converter based on PID regulator is also implemented, and the performance comparison is conducted. As shown in Fig. 15, with the hybrid control method, the HV dc/dc converter has the similar dynamic properties when the motor runs at the same speed, no matter whether the proposed back EMF control strategy is used or not. The adjust time is about 20 ms and the overshoot is zero when the motor runs at 8000 or 21 000 r/min.

The experimental results of different PFCC method of AMB system based on PID control method are shown in Fig. 16. In this case, the HV dc/dc converter has similar dynamic properties when the motor runs at the same speed with different back EMF control strategies. The adjust time is 30 ms and the overshoot is about 4 V when the motor runs at 8000 r/min. However, when the motor runs at 21 000 r/min, the dynamic performance of the HV dc/dc converter is degraded with a shorter adjust time (20 ms) and a larger overshoot (10 V). With different speeds of the motor, the equivalent load, which consists of the AMB bearings and their drives, is also changed. The linear controller such as PID with fixed coefficients is not suitable for the HV dc/dc converter, while the proposed hybrid control method could bring steady control performance with different running conditions of the AMB systems. Furthermore, the coefficients regulation of the PID controller is very dangerous when the motor runs at the rated high speed. If the overshot of output is too large to exceed

the input range of the LV dc/dc converter, the power of the AMB system would also fail.

VI. Conclusion

In this paper, a novel PFCC method of the AMB system is proposed and implemented on a magnetically levitated TMP experimental platform. The principle of this method is converting the kinetic energy of the rotor to the electric power for the AMB system when the mains power fails. The hardware composition is improved to be integrated with the motor drive using either PWM or PAM techniques.

In order to minimize the touchdown damage and improve the efficiency of the energy conversion, an active control strategy of the line-to-line back EMF is used when the motor speed is low. Unlike traditional PWM rectified technique, only six discrete positions are needed which makes it suitable for the PM motor drive using low-revolution position sensors or sensorless control strategy. With a simple PI controller, the feedback power from the motor can be regulated to supply a fixed voltage as input for the buck converter. In addition, an improved digital controller combined SMC with PID algorithm is also introduced to improve dynamic response of the buck converter. Experiment results show that this novel PFCC method can effectively prevent the rotor from touching down the backup bearings at high speed when the mains power fails. The reliability of AMB system can be greatly improved by integrating this PFCC method with the motor drive algorithm.

References

[1] Y. Ren, D. Su, and J. Fang, "Whirling modes stability criterion for a magnetically suspended flywheel rotor with significant gyroscopic effects and bending modes," *IEEE Trans. Power Electron.*, vol. 28, no. 12, pp. 5890–5901, Dec. 2013.

[2] X. Zhou and J. Fang, "Precise braking torque control for attitude control flywheel with small inductance brushless DC motor," *IEEE Trans. Power Electron.*, vol. 28, no. 11, pp. 5380–5390, Nov. 2013.

[3] J. Fang, X. Zhou, and G. Liu, "Precise accelerated torque control for small inductance brushless DC motor," *IEEE Trans. Power Electron.*, vol. 28, no. 3, pp. 1400–1412, Mar. 2013.

[4] J. Fang and Y. Ren, "Decoupling control of a magnetically suspended rotor in a control moment gyro based on inverse system method," *IEEE/ASME Trans. Mechatronics*, vol. 17, no. 6, pp. 1133–1144, Dec. 2012.

[5] T. Kanematsu, S. Wakui, and Y. Nakamura, "A phase stabilization method for unbalance vibration control of five-axis active magnetic bearing systems," in *Proc. IEEEE/ASME Int. Adv. Intell. Mechatronics*, 2014, pp. 150–155.

[6] M. A. Pichot, J. P. Kajs, B. R. Murphy, A. Ouroua, B. M. Rech, R. J. Hayes, J. H. Beno, G. D. Buckner, and A. B. Palazzolo, "Active magnetic bearings for energy storage systems for combat vehicles," *IEEE Trans. Magn.*, vol. 37, no. 1, pp. 318–323, Jan. 2001.

[7] H. Kanematsu, S. Wakui, and Y. Nakamura, "Analysis and control of one-axis active magnetic bearing using single side electromagnetic drive," in *Proc. IEEEE/ASME Int. Adv. Intell. Mechatronics.*, 2014, pp. 781–787.

[8] K. Y. Zhu, Y. Xiao, and A. U. Rajendra, "Optimal control of the magnetic bearings for a flywheel energy storage system," *Mechatronics*, vol. 19, no. 8, pp. 1221–1235, Dec. 2009.

[9] M. Ahrens, L. Kucera, and R. Larsonneur, "Performance of a magnetically suspended flywheel energy storage device," *IEEE Trans. Control Syst. Technol.*, vol. 4, no. 5, pp. 494–502, Sep. 1996.

[10] G. Schweitzer, *Magnetic Bearings: Theory, Design, and Application to Rotating Machinery*. Berlin, Germany: Springer-Verlag, 2009.

[11] T. Ishii and R. G. Kirk, "Transient response technique applied to active magnetic bearing machinery during rotor drop," *ASME J. Vibration Acoust.*, vol. 118, no. 2, pp. 154–163, Apr. 1996.

[12] I. Kim, "A technique for estimating the state of health of lithium batteries through a dual-sliding-mode observer," *IEEE Trans. Power Electron.*, vol. 25, no. 4, pp. 1013–1022, Apr. 2010.

[13] M. Bragard, N. Soltau, S. Thomas, and R. W. De Doncker, "The balance of renewable sources and user demands in grids: Power electronics for modular battery energy storage systems," *IEEE Trans. Power Electron.*, vol. 25, no. 12, pp. 3049–3056, Dec. 2010.

[14] S. Vazquez, S. M. Lukic, E. Galvan, L. G. Franquelo, and J. M. Carrasco, "Energy storage systems for transport and grid applications," *IEEE Trans. Ind. Electron.*, vol. 57, no. 12, pp. 3881–3895, Dec. 2010.

[15] D. Linden and T. B. Reddy, *Handbook of Batteries*. New York, NY, USA: McGraw-Hill, 2002.

[16] Koyo Seiko Co., Ltd., "Magnetic bearing control device," U.S. Patent 6 617 734 B2, 2003.

[17] Siemens Aktiengesellschaft, "Device for safeguarding an uninterruptible power supply of a magnet bearing in the event of failure of an electrical supply voltage," U.S. Patent 7 928 620 B2, 2011.

[18] D. J. You, S. M. Jang, J. P. Lee, and T. H. Sung, "Dynamic performance estimation of high-power FESS using the operating torque of a PM synchronous motor/generator," *IEEE Trans. Magn.*, vol. 44, no. 11, pp. 4155–4158, Nov. 2008.

[19] C. Xiaoyong, L. Yongli, Z. Weiya, W. Nan, and X. Wei, "Active disturbance rejection control for a flywheel energy storage system," *IEEE Trans. Ind. Electron.*, vol. 62, no. 2, pp. 991–1001, Feb. 2015.

[20] G. O. Cimuca, C. Saudemont, B. Robyns, and M. M. Radulescu, "Control and performance evaluation of a flywheel energy-storage system associated to a variable-speed wind generator," *IEEE Trans. Ind. Electron.*, vol. 53, no. 4, pp. 1074–1085, Jun. 2006.

[21] D. H. Braun, T. P. Gilmore, and W. A. Maslowski, "Regenerative converter for PWM AC drives," *IEEE Trans. Ind. Appl.*, vol. 30, no. 5, pp. 1176–1184, Sep./Oct. 1994.

[22] J. C. Schroeder and F. W. Fuchs, "General analysis and design guideline for a battery buffer system with DC/DC converter and EDLC for electric vehicles and its influence on efficiency," *IEEE Trans. Power. Electron.*, vol. 30, no. 2, pp. 922–932, Mar. 2014.

[23] M.-J. Yang, H.-L. Jhou, B.-Y. Ma, and K.-K. Shyu, "A cost-effective method of electric brake with energy regeneration for electric vehicles," *IEEE Trans. Ind. Electron.*, vol. 56, no. 6, pp. 2203–2212, Feb. 2009.

[24] X. Nian, F. Peng, and H. Zhang, "Regenerative braking system of electric vehicle driven by brushless DC motor," *IEEE Trans. Ind. Electron.*, vol. 61, no. 10, pp. 5798–5808, Jan. 2014.

[25] NTN Co., "Power supply circuit for magnetic bearing system," U.S. Patent 5574345 A, 1996.

[26] Turbocor, Inc., "Power supply circuit of a high speed electric motor," U.S. Patent 7116066 B2, 2006.

[27] L. Kwanghwa and F. C. Y. Lee, "Zero-voltage switching technique in DC/DC converters," *IEEE Trans. Power Electron.*, vol. 5, no. 3, pp. 293–304, Jul. 1990.

[28] W. Tang, F. C. Lee, and R. B. Ridley, "Small-signal modeling of average current-mode control," *IEEE Trans. Power Electron.*, vol. 8, no. 2, pp. 112–119, Apr. 1993.

[29] D. C. Hamill, J. H. B. Deane, and D. J. Jeffries, "Modeling of chaotic DC-DC converters by iterated nonlinear mappings," *IEEE Trans. Power Electron.*, vol. 7, no. 1, pp. 25–36, Jan. 1992.

[30] A. M. Rahimi, M. H. Alavi, and M. R. Zolghadri, "A precise large signal model for a flyback converter in critical conduction mode," in *Proc. IEEE Int. Power Electron. Drive Syst.*, 2001, pp. 886–891.

[31] S. Chattopadhyay and S. Das, "A digital current-mode control technique for DC–DC converters," *IEEE Trans. Power Electron.*, vol. 21, no. 6, pp. 1718–1726, Nov. 2006.

[32] G. Feng, E. Meyer, and Y. F. Liu, "A new digital control algorithm to achieve optimal dynamic performance in DC-to-DC converters," *IEEE Trans. Power Electron.*, vol. 22, no. 4, pp. 1489–1498, Jul. 2007.

[33] T. Siewchong, L. Yukming, and T. Chikong, *Sliding Mode Control of Switching Power Converters Techniques and Implementation*. Boca Raton, FL, USA: CRC Press, 2011.

[34] L. G. Shiau and J. L. Lin, "Direct and indirect SMC control schemes for DC–DC switching converters," in *Proc. 36th SICE Annu. Conf. Int. Session Papers*, Jul. 1997, pp. 1289–1294.

[35] Y. F. Liu, E. Meyer, and X. Liu, "Recent developments in digital control strategies for DC/DC switching power converters," *IEEE Trans. Power Electron.*, vol. 24, no. 11, pp. 2567–2577, Nov. 2009.

[36] C. Cui, G. Liu, K. Wang, and X. Song, "Sensorless drive for high-speed brushless DC motor based on the virtual neutral voltage," *IEEE Trans. Power Electron.*, vol. 30, no. 6, pp. 3275–3285, Jul. 2014.

[37] C. Cui, G. Liu, and K. Wang, "A novel drive method for high-speed brushless DC motor operating in a wide range," *IEEE Trans. Power Electron.*, vol. 30, no. 9, pp. 4998–5008, Oct. 2014.
[38] Y. Li, K. H. Ang, and G. C. Y Chong, "PID control system analysis and design," *IEEE Control Syst. Mag.*, vol. 26, no. 1, pp. 32–41, Feb. 2006.

Gang Liu received the B.S. degree from Shandong University, Jinan, China, in 1992, the M.S. degree from Shandong University, Jinan, in 1998, and the Ph.D. degree from the Dalian University of Technology, Dalian, China, in 2001.

He is currently with the School of Instrument Science and Optoelectronic Engineering, BeiHang University, Beijing, China, as a Ph.D. Supervisor. His research interests include permanent magnet motor control, spacecraft attitude control, and electrical control systems.

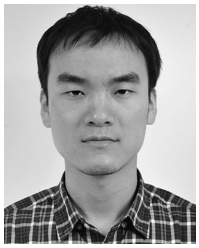

Kun Mao received the B.S. degree from the Southwest University of Science and Technology, Mianyang, China, in 2009, the M.S. degree from BeiHang University, Beijing, China, in 2012. He is currently working toward the Ph.D. degree in the School of Instrumentation Science and Optoelectronics Engineering, BeiHang University.

He is also a Research Member of the Key Laboratory of Fundamental Science for National Defense, Novel Inertial Instrument and Navigation System Technology. His research interests include power electronics and high-speed permanent magnet motor control.